

KAN-Therm: A Lightweight Battery Thermal Model Using Kolmogorov-Arnold Network

A PREPRINT

Soumyoraj Mallick ^{*,1}, Sanchita Ghosh ^{*,1}, and Tanushree Roy¹

¹Department of Mechanical Engineering, Texas Tech University, Lubbock, TX 79409, US.

Emails: somallic@ttu.edu, sancghos@ttu.edu, tanushree.roy@ttu.edu.

September 12, 2025

ABSTRACT

Battery management systems (BMSs) rely on real-time estimation of battery temperature distribution in battery cells to ensure safe and optimal operation of Lithium-ion batteries (LIBs). However, physical BMS often suffers from memory and computational resource limitations required by high-fidelity models. Temperature prediction using physics-based models becomes challenging due to their higher computational time. In contrast, machine learning based approaches offer faster predictions but demand larger memory overhead. In this work, we develop a lightweight and efficient Kolmogorov-Arnold networks (KAN) based thermal model, KAN-Therm, to predict the core temperature of a cylindrical battery. We have compared the memory overhead and computation costs of our method with Multi-layer perceptron (MLP), recurrent neural network (RNN), and long short-term memory (LSTM) network. Our results show that the proposed KAN-Therm model exhibit the best prediction accuracy with the least memory overhead and computation time.

1 Introduction

Reliable operation of Lithium-ion batteries (LIBs) play a crucial role in ensuring the efficient operation of renewable energy-based infrastructure systems, including smart grids and electric vehicles [1]. This reliability is heavily dependent on the operating temperature of the LIBs, and effective thermal management can ensure optimal battery operation with improved longevity while preventing overheating [2]. However, unlike the surface temperature, the core temperature of the battery is often inaccessible, thus estimating the temperature distribution within the battery cell is critical to ensure safety [3]. While high-fidelity thermal model-based H_∞ observers [4] and Kalman-filters [3] have been adopted for core temperature estimation, these methods are not well suited for practical application due to their high computational demand, parameterization difficulty, and poor observability issues [5, 6]. Therefore, recent LIB research has focused on developing advanced machine learning (ML) algorithms to capture the thermal behavior of LIBs [2].

For instance, [7] developed three high-performing ML models for core temperature estimation based on recurrent neural network (RNN), long short-term memory (LSTM) network, and gated recurrent unit (GRU) network. Similarly, [5] proposed a LSTM-RNN-based model to generate real-time estimation of average battery temperature. Accordingly, [8] developed a LSTM-based model for predicting instant battery temperature as well as for forecasting long-term thermal fluctuations in battery to capture any early warning signs of thermal anomalies. [9] deployed separate LSTM models for each cell in a battery pack to generate parallel cell temperature estimation for reliable thermal runaway prediction. On the other hand, [10] proposed a bank of seasonal nonlinear autoregressive exogenous NN models considering multiple models corresponding to the weather-characteristics in each season for cell temperature estimation. Furthermore, [11] integrated LSTM model with transfer learning for core temperature prediction while reducing data requirement and to facilitating adaptability across different LIBs.

^{*}These authors contributed equally to this work.

Several works have also utilized hybrid models to combine the data-driven methods with the physic-based models [12]. An unscented Kalman-filter (KF) was integrated with the NN model to generate accurate core temperature estimation with experimental validation in [13]. Similarly, [14] proposed a noise compensated extended KF for core temperature estimation where they utilized a NN model to characterize the model noises from available sensor data. In [12], a two-dimensional grid LSTM model was adopted, where the model-based heat generation estimation was incorporated as one of the input features to improve the core temperature estimation performance further. ML methods (artificial NN (ANN) [15] and convolutional NN (CNN) combined with the artificial bee colony optimization technique [16]) have been also adopted for such heat generation rate estimation in LIB cells. Furthermore, to obtain reduced model-complexity in the hybrid models, [17] utilized numerical techniques to simplify the thermal model, and then fused the numerical model with a LSTM network for core temperature estimation.

In addition to the above mentioned ML methods, Kolmogorov Arnold Network (KAN) is becoming increasingly popular in the battery community [18]. [19] has shown that the KAN model outperforms ANN and barnacles mating optimizer-deep learning models in battery state-of-charge (SOC) estimation. Moreover, hybrid CNN-KAN model [20], Kolmogorov-Arnold-Linformer (KAL) network model [21], and KAN model integrated with dynamic-graph-generator [22] have been explored for predicting battery state-of-health (SOH) with improved accuracy while utilizing the learnable activation functions of KAN to enhance the model's robustness, flexibility, and the capability for nonlinear features representation. Similarly, [23] combined KAN with a lightweight GRU network to enhance the generalization and feature extraction capability of the GRU, leading to an improved performance in remaining useful life estimation for the LIB. [18] combined KAN with a squeeze-and-excitation module for predicting the capacity degradation of electric vehicle battery packs, where the KAN module improved the model's adaptability to changes in charging data.

This success of KAN for LIB state estimation motivates our research. Additionally, [2] explored the KAN model for LIB thermal modeling and core temperature estimation and points out the need for further research work and development for KAN implementation. In particular, [2] focused on estimating the core temperature of LIBs without surface temperature feedback, but at the cost of a heavy network architecture with higher computational demand. Thus, there is a clear gap to develop a lightweight KAN structure for LIB thermal modeling, by leveraging nonlinear feature learning capabilities of KAN via small structure [24].

The reduced model storage overhead are required for small compute physical BMS that are essential for applications such as health monitoring devices, embedded electronics [25]. Furthermore, lighter models at the cell level will enable model scaling to the pack level, leading to a more realistic and easily deployable framework. Lighter models with simple network structures can also deliver faster model prediction, which is needed for safety-critical performance and system diagnostics. Thus, in this work, our primary *contribution* is to train a lightweight KAN-Thermal model, and with better accuracy and faster prediction times than the state-of-the-art models for cylindrical cells.

The rest of the paper is organized as follows. Section 2 presents the preliminaries and theoretical background for KAN. The proposed KAN-Therm model development and training are described in Section 3. We present the detailed results of our tests and performance comparison in Section 4. Finally, in Section 5 we conclude our work.

2 Preliminaries On Kolmogorov-Arnold Network

Kolmogorov-Arnold network (KAN) [24] is built upon the Kolmogorov-Arnold representation theorem, which states that a multivariate continuous function can be expressed as a finite number of compositions of univariate continuous functions and the addition operation. While the theorem asserts the existence of such univariate functions, their construction is not straightforward. KAN utilizes an L -deep multi-layer network structure to learn these functions, where each layer has W_l number of nodes and each node represents a single variable $x_{l,w}$, $\forall w \in \{1, \dots, W_l\}$, $l \in \{1, \dots, L\}$. W_l here represents the width of each layer l . At each KAN-layer l , the value $x_{l,w}$ at every node is passed through an activation function $\theta_{l,w^+,w}$, $\forall w^+ \in \{1, \dots, W_{l+1}\}$ which are then added to produce the node value at each node w^+ in the consecutive layer $l+1$. This can be written as

$$x_{l+1,w^+} = \sum_{w=1}^{W_l} \theta_{l,w^+,w}(x_{l,w}), \forall w^+ \in \{1, \dots, W_{l+1}\}. \quad (1)$$

In a compact matrix form, it can be expressed as,

$$x_{l+1} = \underbrace{\begin{pmatrix} \theta_{l,1,1}(\cdot) & \dots & \theta_{l,1,W_l}(\cdot) \\ \vdots & \ddots & \vdots \\ \theta_{l,W_{l+1},1}(\cdot) & \dots & \theta_{l,W_{l+1},W_l}(\cdot) \end{pmatrix}}_{\Theta_l} x_l, \quad (2)$$

where the activation function matrix at layer l is given by Θ_l and the node vector at layer l is denoted by x_l , $\forall l$. The goal of a multi-layer KAN architecture is to learn these activation functions $\Theta_l \forall l$ to capture the relationship between N_1 input variables (or feature variables) denoted by $x_1 = [x_{1,1}, \dots, x_{1,N_1}]$ and N_{L+1} output variables (or target/prediction variables) denoted by x_o . Mathematically, this can be represented as $x_o = KAN(x_1) = (\Theta_L \circ \Theta_{L-1} \circ \dots \circ \Theta_1)x_1$. In this work, we use a sum of silu function and a linear combination of k -order B-splines over G grid points to represent our activation functions $\theta_{l,w^+,w}$. The weights for the spline combination and the "fine-graining" of the grid are learned using backpropagation and gradient descent using the loss function defined below.

Loss function: The loss function ℓ_{total} used for KAN training is defined to reduce prediction error and the number of parameters of KAN model such that a lightweight structure is realized by prioritizing dominant activation functions [24]. The first objective is captured using a mean squared prediction error ℓ_{pred} between predicted and true output. The sparsification of the KAN model to reduce the parameter count is realized by minimizing the l_1 -norm contribution of the activation functions ($|\Theta_l|_1$) (4) with a self-entropy term $S(\Theta_l)$ (5). The total loss function is then represented by

$$\ell_{total} = \ell_{pred} + \lambda \left(\nu_1 \sum_{l=0}^{L-1} |\Theta_l|_1 + \nu_2 \sum_{l=0}^{L-1} S(\Theta_l) \right), \quad (3)$$

$$|\Theta_l|_1 = \sum_{w=1}^{W_l} \sum_{w^+=1}^{W_{l+1}} |\theta_{w,w^+}|_1, \quad (4)$$

$$S(\Theta_l) = - \sum_{w=1}^{W_l} \sum_{w^+=1}^{W_{l+1}} \frac{|\theta_{w,w^+}|_1}{|\Theta_l|_1} \log \left(\frac{|\theta_{w,w^+}|_1}{|\Theta_l|_1} \right), \quad (5)$$

where the sparsification penalty term λ and regularization terms ν_1, ν_2 are the hyperparameters of the model.

Parameter count: The total number of parameters in KAN network is given by $\mathcal{O}(\sum_{l=1}^L W_l^2(G+k))$, for a network having depth L and each spline is of order k over G intervals or for $(G+1)$ grid points.

We note here that a standard neural network architecture, in contrast, is based on approximating functions of multiple variables (or input features) as *learnable* linear transformations of node values through *weights* and their subsequent transformation via *fixed nonlinear activation functions*.

3 Introduction to KAN-Therm Model

In this section, we develop our KAN-Therm model to estimate the core temperature (\hat{T}_1) of the battery. We also discuss the data generation strategy for the training, validation, and testing of the model using a battery lumped thermal model. The details of the training procedure and hyperparameter selection have also been highlighted.

3.1 Battery thermal model

To generate the battery data for this work, we adopt a lumped parameter thermal model of a cylindrical LIB cell with a cooling system placed at the surface of the cell [26, 27]. The governing equations for the core temperature (T_1), surface temperature (T_2) of the cell and coolant temperature (T_∞) of the cooling system are given by,

$$\dot{T}_1(t) = -\frac{T_1(t) - T_2(t)}{R_1 C_1} + \frac{\dot{Q}(t)}{C_1}, \quad (6)$$

$$\dot{T}_2(t) = -\frac{T_2(t) - T_1(t)}{R_1 C_2} - \frac{T_2(t) - T_\infty(t)}{R_2 C_2}, \quad (7)$$

$$\dot{T}_\infty(t) = -\frac{T_\infty(t) - T_2(t)}{R_2 C_\infty} - \frac{\dot{Q}_c(t)}{C_\infty}, \quad (8)$$

where R_1 and R_2 are the thermal resistances between battery core and surface and between surface and coolant, respectively, C_1 , C_2 and C_∞ are the heat capacities of the battery material at core, at surface and of cooling system, respectively, \dot{Q}_c represents cooling power of the cooling system, and \dot{Q} is the heat generation term.

Heat generation \dot{Q} inside the cell is related to its electrical behavior and can be modeled as,

$$\dot{Q}(t) = I(t) \left(V_{\text{OCV}}(\text{SOC}) - V_t(t) - T_1(t) \mathbb{E} \right), \quad (9)$$

where I is the current through the battery, V_{OCV} is the open circuit voltage as a function of SOC, V_t is the terminal voltage, and \mathbb{E} is the entropic heat coefficient of the LIB cell. The SOC dynamics and terminal voltage V_t of the battery is given by,

$$\dot{\text{SOC}}(t) = -\frac{I(t)}{Q_b}, \quad V_t(t) = V_{\text{OCV}}(\text{SOC}) - I(t)R_s. \quad (10)$$

Here, Q_b is the battery capacity and R_s is the electrical resistance [28]. Using (10), we can rewrite $\dot{Q} = -I^2 R_s - I T_1 \mathbb{E}$.

3.2 Data generation

For this study, we consider a 2.3Ah cylindrical $\text{LiFePO}_4 - \text{LiC}_6$ battery cell where the thermal parameters for (6)-(10) have been adopted from [29, 30], and the left column of Table 1 lists the parameter. We use numerical integration on MATLAB 2024a on the lumped parameter thermal model (6)-(10) to collect the training, validation, and testing data under different scenarios of battery charging-discharging conditions. The dynamic current profiles included benchmark profiles of the Urban Dynamometer Driving Schedule (UDDS) [31], the Supplemental Federal Test Procedure (US06) [32], and automotive battery cycle [33]. The constant current (CC) profiles varied from 1C-rate (2.3A) to 3C-rate (6.9A). Moreover, the dataset considers variations in coolant power \dot{Q}_c , initial SOC, and the initial battery temperatures (i.e. ambient temperature). In total, time series datasets from 19 distinct scenarios have been obtained and 74% of this data has been used to train the KAN-Therm model, 16% data to validate, and 10% data for testing the performance of the proposed KAN-Therm model (see Fig. 1). The testing dataset includes data under CC charging at 1C-rate and a scaled UDDS cycle. Furthermore, to simulate realistic sensor measurements, white Gaussian noise with a standard deviation of 0.5% has been added to the data. The histogram in Fig. 2 shows the number of training data distributed across different ranges of current and core temperature of the battery.

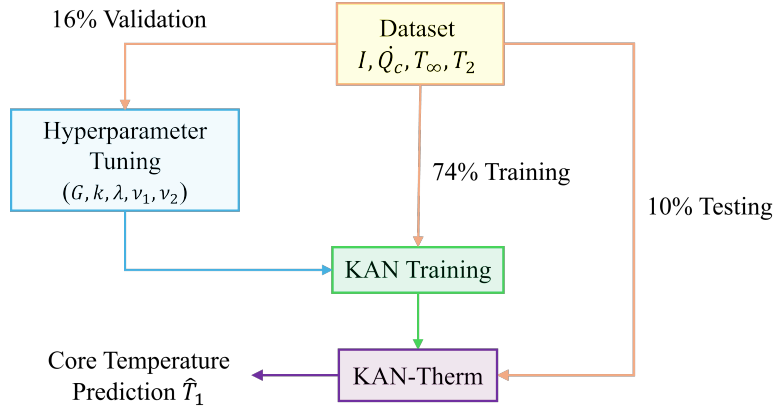


Figure 1: Flowchart shows how the dataset is split into training, validation, and testing subsets.

3.3 Model development

The proposed KAN-Therm model incorporates 4 input features: the applied current I , the cooling power \dot{Q}_c , the temperature of the cooling system T_∞ , and the surface temperature of the battery T_2 . These variables can be readily measured and are assumed to be known. Our goal in training the KAN-Therm model is to learn the activation functions such that $\hat{T}_1 = \text{KAN}(I, \dot{Q}_c, T_\infty, T_2)$, based on the training data generated (as described in the last subsection). Fig. 3 shows the block diagram of the proposed KAN-Therm model, with its input features and output.

For our KAN-Therm model, the four input variables I, \dot{Q}_c, T_∞ , and T_2 are input nodes of the 1st layer of width $N_1 = 4$. Next, we consider a KAN layer of width $N_2 = 3$ to finally produce the output- the core temperature prediction \hat{T}_1 . Thus, we have a network configuration of $\llbracket 4, 3, 1 \rrbracket$ for the KAN-Therm model. In this architecture, 12

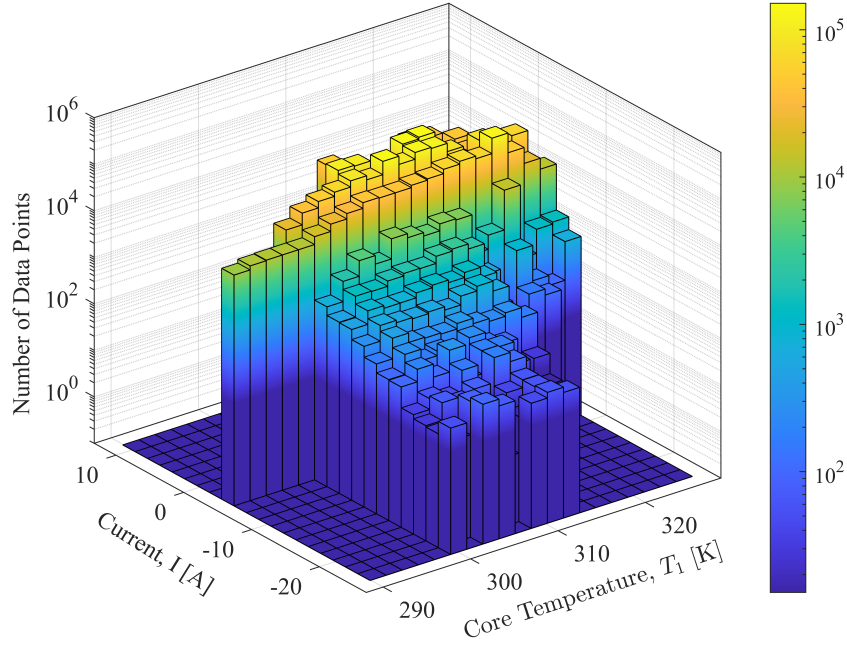


Figure 2: Data distribution of current (I) vs core temperature (T_1).

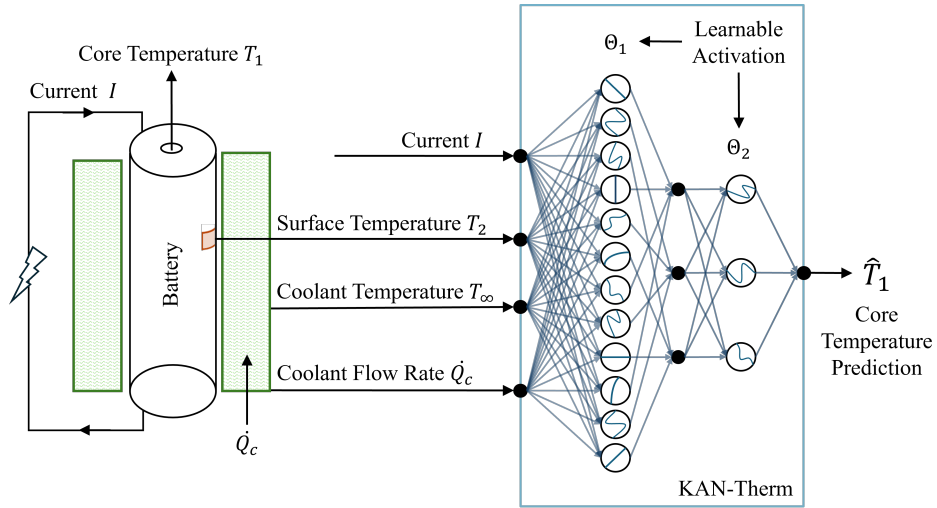


Figure 3: Block diagram illustration of the proposed KAN-Therm model for prediction of battery core temperature (\hat{T}_1).

learnable activation functions are present in the 1st KAN layer, while 3 are present in the 2nd KAN layer. To train the KAN-Therm model, the complete dataset has been normalized between 0 to 1 range using min-max normalization. Furthermore, to efficiently optimize the minimization of the loss function, L-BFGS optimizer has been used during training.

Hyperparameter tuning: We adopt the *grid search* approach to obtain the best-suited set of hyperparameters that yields the optimal KAN-Therm model that minimizes our pre-defined loss function ℓ_{total} (3) on our validation datasets. Grid search is a brute-force or exhaustive way of searching through a manually specified subset of the hyperparameter space such that the subset is defined within lower- and higher-bounds along with specific steps [34]. During our

hyperparameter tuning, we grid search for nine hyperparameters of the KAN-Therm model, as described in five groups below.

(i) *Network width for KAN layers* affects the model complexity as well as the learning capability. As part of our hyperparameter search, the width of the 2nd KAN layer ($l = 2$) is varied over the values $\{2, 3, 4, 5, 6\}$. While we tested KAN structures with more than 2 layers (as presented in this paper), all those KAN structures produced similar or poorer accuracy with considerable increase in parameter count and training time. We have not presented the analysis of those structures in this paper for the brevity of presentation.

(ii) *Spline order k & grid interval G* significantly influence the nonlinear feature representation capability of the model. For both of these hyperparameters, the model performance is tested over the set $\{2, 3, 4, 5, 6\}$. The results of the grid search produce the best model for $k = 3$ and $G = 5$.

(iii) *Sparsification parameters λ, ν_1, ν_2* ensure parameter reduction of the model by suppressing weaker activations. During grid search, we consider the set $\{0.01, 0.001, 0.0025, 0.0005, 0.0001\}$ for λ and the set $\{0.1, 0.25, 0.5, 0.75, 1\}$ for both ν_1, ν_2 . Based on our grid search result, we choose $\lambda = 0.0001, \nu_1 = \nu_2 = 0.25$ to obtain the best accuracy, while maintaining the lightweight structure for the model.

(iv) *Total number of epochs & early stopping of the spline grid update* impact the model convergence and control the chances of overfitting. During our model training, we monitor the convergence of training and the validation loss over a set of epoch choices $\{25, 50, 75, 100, 125, 150, 175, 200\}$ to obtain the best model performance for 150 epochs. Similarly, the spline grid update hyperparameter controls the number of epochs over which the spline grid range is updated to minimize the loss function. During model training, we consider the set of spline grid update choices of $\{25, 50, 75, 100, 125, 150\}$ epochs and obtained the best accuracy without overfitting for stopping the spline grid update within the first 50 epochs.

(v) *Training batch size* affects the convergence, computational speed, and resource requirement during training. The batch size during our model training is finalized as $1E5$ after searching through the set of batch size choices $\{128, 1E4, 5E4, 7.5E4, 1E5, 2E5, 3E5\}$ for $aEb = a \times 10^b$.

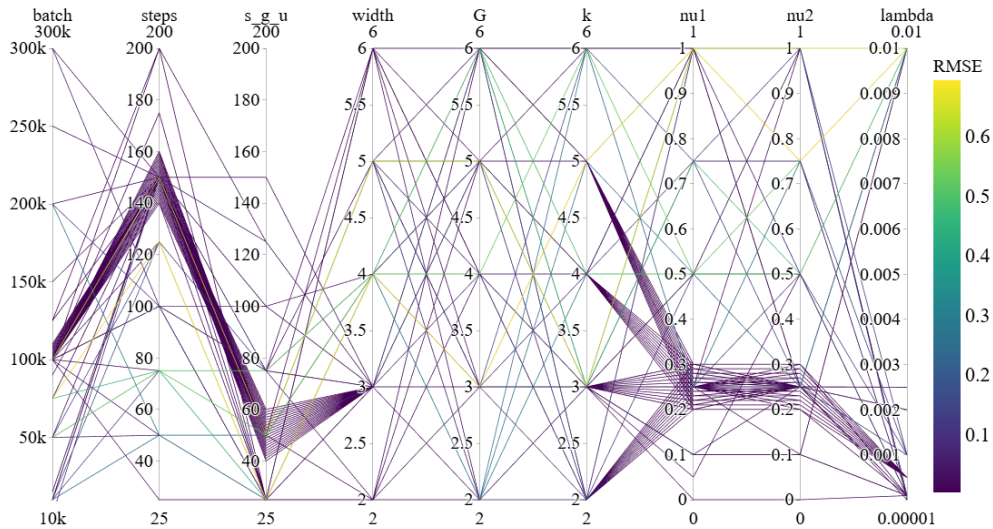


Figure 4: Parallel coordinate plot illustrates the exploratory findings of the hyperparameter tuning process for our proposed KAN-Therm model.

The parallel coordinate plot in Fig. 4 depicts our rigorous hyperparameter exploration findings that finally enabled us to obtain a lightweight KAN-Therm model. In Fig. 4, each vertical axis represents a hyperparameter, and each line represents the hyperparameter combinations in a single run of the model. Additionally, the color of each line maps the validation loss for the particular run to visually illustrate the model performance with different combinations of hyperparameters. Based on our analysis, we choose the hyperparameter combination that yields the best model performance with a final loss of $2.5E - 3$ and $2.6E - 3$, respectively, for training and validation. Table 1 captures the finalized hyperparameters used during the training process. Fig. 5 shows that the training and validation losses converge without overfitting during training of the KAN-Therm model. Next, we evaluate the performance of our

Battery Simulation Parameters		KAN Hyperparameters	
Parameters	Values	Parameters	Values
R_1	$1.61 \text{ } KW^{-1}$	Network width	$\llbracket 4, 3, 1 \rrbracket$
R_2	$3.14 \text{ } KW^{-1}$	G	5
C_1	$59.50 \text{ } JK^{-1}$	k	3
C_2	$4.40 \text{ } JK^{-1}$	λ	0.0001
C_∞	$10.00 \text{ } JK^{-1}$	ν_1	0.25
\mathbb{E}	$10^{-4} \text{ } WK^{-1}$	ν_2	0.25

Table 1: Battery simulation and KAN-Therm model parameters

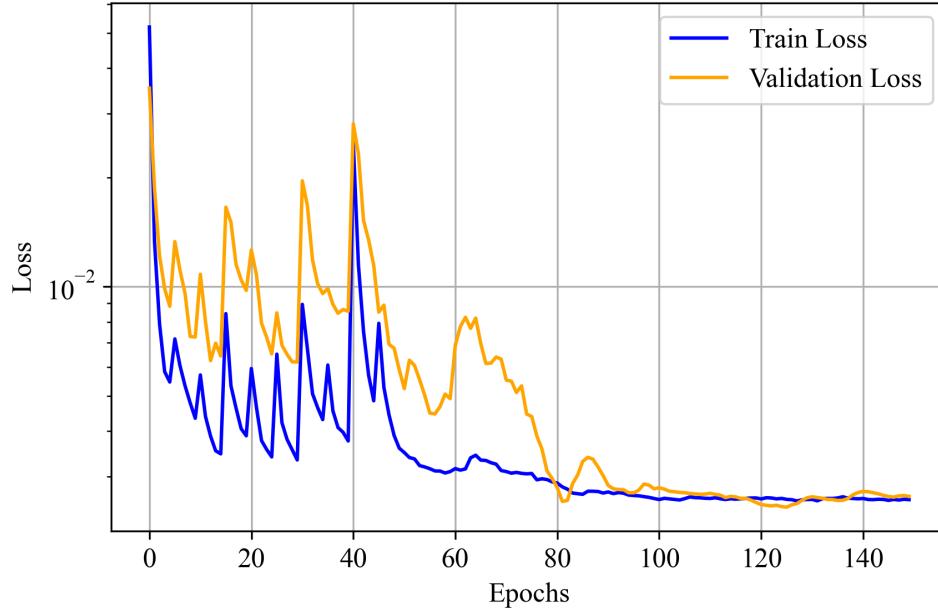


Figure 5: Figure shows the training and validation loss with epochs for the KAN-Thermal model.

proposed KAN-Therm model as well as highlight its advantages over state-of-the-art ML networks, specifically in deployability on a resource-constrained physical BMS.

4 Performance Tests And Comparison

In this section, we present the test results comparing the performance of the proposed KAN-Therm model against three benchmark ML networks namely MLP, RNN, and LSTM. This comparison provided us with a well-rounded assessment of the KAN-Therm model’s predictive performance and memory- & compute- requirements.

4.1 Baseline methods: MLP, RNN, & LSTM

We consider three baseline neural network models for comparison with the proposed KAN-Therm model, while considering three performance criteria: prediction accuracy, model complexity or parameter counts, and prediction time. We thoroughly explored the hyperparameter space for each baseline method using extensive grid search and compared their best performance with our proposed KAN-Therm model. Furthermore, we use ReLU activation function along with the Adam optimization technique in all the baseline models to mitigate the risks of vanishing gradients for faster and accurate training [35].

MLP is a type of feedforward neural network consisting of fully-connected layers [21]. Our baseline MLP is chosen as $\llbracket 4, 10, 10, 1 \rrbracket$ i.e., there are 4 neurons in the input layer, 10 neurons in each of the two hidden layers, and a single output neuron.

RNN is tailored for sequential data processing that contains neural networks with recurrent units, a form of memory that is updated at each time step based on the current input and the hidden state from the previous step [7]. In this study, we consider an RNN network of $\llbracket 4, 15, 25, 5, 1 \rrbracket$, representing a recurrent layer with 15 memory units and two fully connected hidden layers with 25 and 5 neurons, respectively. Furthermore, we choose a lookback window of 20 data points for the RNN model through the hyperparameter search.

LSTM is a variant of RNN that can address the issue of long-term dependency and learns to store and discard information selectively for efficient learning of sequential data [7]. LSTM includes one cell and three gates: forget gate, input gate, and output gate such that the cell state holds the values for arbitrary time interval, while the forget gate removes information that is no longer needed in the cell state, the input gate adds information that is useful in the cell state, and the output gate extracts useful information from the current cell state to be presented as output [7]. For our study, we consider an LSTM network of $\llbracket 4, 4, 8, 2, 1 \rrbracket$ which represents one LSTM layer with 4 LSTM units followed by two fully connected hidden layers consisting 8 and 2 neurons, respectively. For the LSTM model, we consider a lookback window of 50 data points based on our hyperparameter search.

4.2 Results & comparison

We tested each method using our generated test dataset that contains both CC charging data and a dynamic UDDS current cycle data. Fig. 6 and Fig. 7 illustrate the test results under CC and UDDS charging conditions, respectively. The top plots of Fig. 6 and Fig. 7 show the true core temperature T_1 (obtained from numerical integration of thermal model in MATLAB) along with the predicted core temperature \hat{T}_1 using KAN-Therm and the three baseline models. The corresponding prediction errors (absolute difference between true and predicted values) are shown in the bottom plots of Fig. 6 and Fig. 7. The zoomed inset of the error plots indicates that KAN-Therm and MLP have comparable errors while RNN and LSTM have comparable but higher prediction errors. Next, we present the detailed analysis of

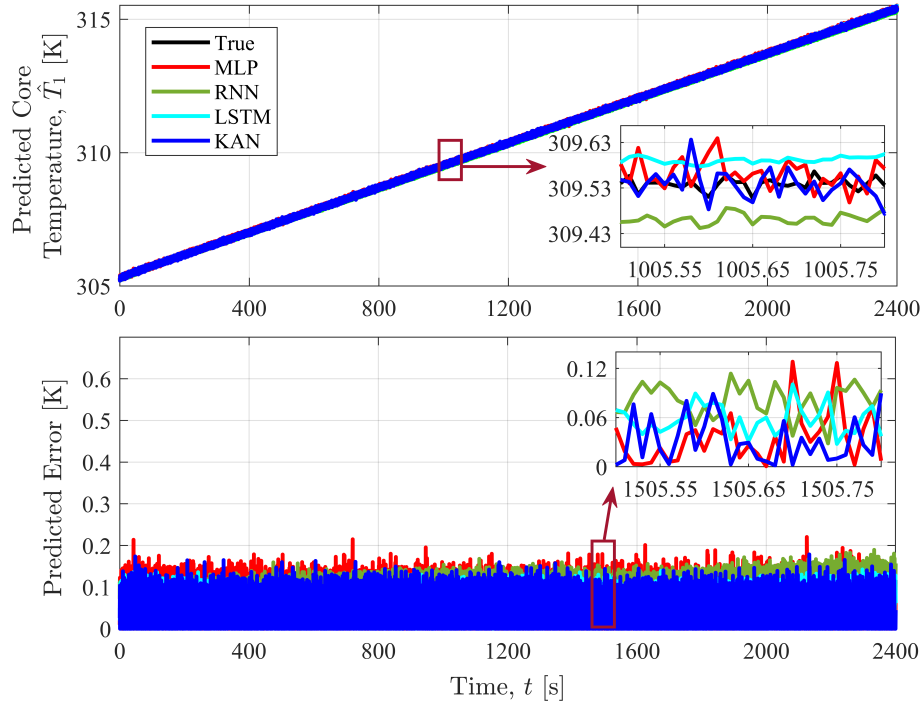


Figure 6: Under CC charging, top plot shows the true core temperature T_1 and the predicted core temperature \hat{T}_1 from four models; the bottom plot presents the corresponding prediction error.

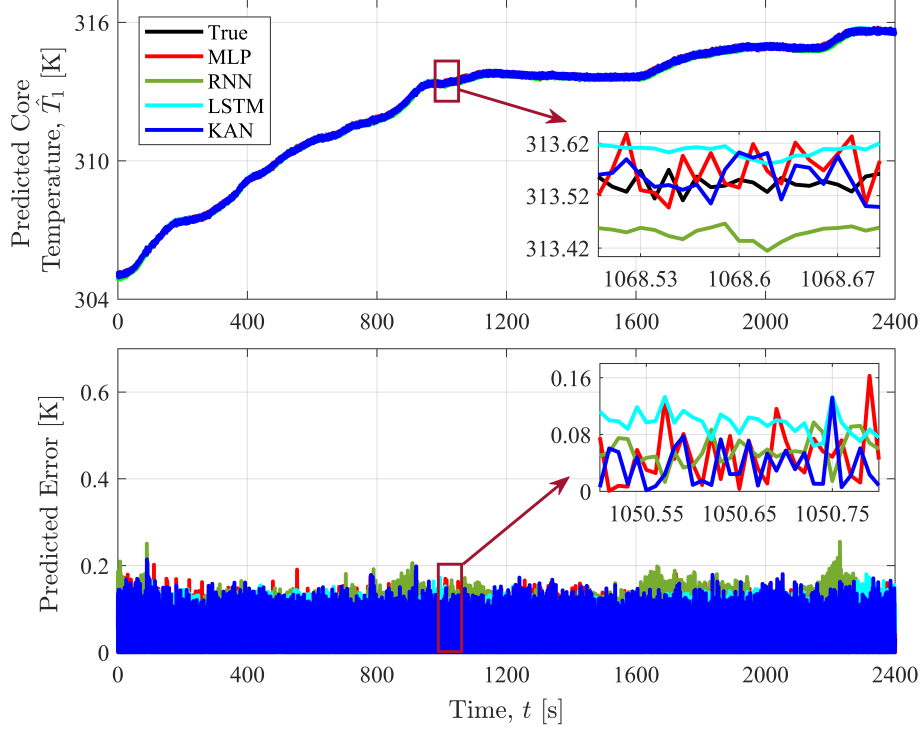


Figure 7: Under UDDS charging, top plot shows the true core temperature T_1 and the predicted core temperature \hat{T}_1 from four models; the bottom plot presents the corresponding prediction error.

the performances of KAN-Therm and the three baseline methods with respect to three criteria: predictive accuracy, number of parameters, and computational run-time for prediction.

Criterion 1: Predictive accuracy The RNN model achieved a prediction RMSE of 0.0832 and LSTM yielded a slighted lower RMSE of 0.0718. These results are congruent with the findings observed in recent works as given in [7], where they estimated the core temperature and achieved 0.079 and 0.076 RMSE for RNN and LSTM, respectively. Our proposed KAN-Therm model outperformed these ML models by achieving the lowest RMSE 0.0368. This prediction accuracy is 11% better than MLP, 56% better than RNN, and 48% better than LSTM. We used the physics-based model as our ground truth, so its accuracy has been excluded from the scope of the performance evaluation.

Criterion 2: Number of parameters: To attain the above-mentioned accuracy levels, RNN required the highest number of parameters of 836, followed by LSTM that required 288 parameters, and MLP required 171 parameters. In contrast, KAN-Therm required only 120 parameters. This result implies that compared to the KAN-Therm model, MLP requires $1.4\times$ more, LSTM requires $2.4\times$ more, and RNN $7.1\times$ more parameters to effectively capture the intrinsic patterns in the data, making it the most lightweight among the tested models. The physics-based model requires only 9 parameters from the battery dynamics to generate the data. This reduced data requirement is the advantage of physics-based modeling.

Criterion 3: Prediction time: Computational run-time of each method was assessed by measuring the time required to predict \hat{T}_1 for 1000 data points. Due to the model weight and complexity of gated architecture, LSTM was the slowest, taking 42ms. RNN performed faster than LSTM, completing the prediction in 35ms. MLP, with its simple network structure, was significantly faster than both LSTM and RNN and required 1.5ms. Our proposed KAN-Therm model exhibited the highest computational speed with a prediction time of only 1.1ms. Thus, the KAN-Therm model generates prediction $1.3\times$, $31.8\times$, and $38.2\times$ faster than MLP, RNN, LSTM, respectively. Additionally, the physics-based model takes 13ms for the data generation. This implies that the proposed KAN-Therm model exhibits $11.8\times$ faster prediction generation compared to the physics-based model.

Table 2 summarizes the comparison results described above. It is evident from Table 2 that the proposed KAN-Therm model provides the highest accuracy with the fastest prediction time compared to the three state-of-the-art ML models and use significantly fewer parameters compared to other state-of-the-art ML models. Thus, our proposed KAN-Therm

model emerges as the most suitable candidate to predict the core temperature of a cylindrical LIB if implemented in a resource-constrained physical BMS.

	Models				
	Physics	MLP	RNN	LSTM	KAN
RMSE [K]	-	0.0415	0.0832	0.0718	0.0368
Parameters	9	171	836	288	120
Prediction Time [ms]	13	1.5	35	42	1.1

Table 2: Summary of performance comparison between the proposed KAN-Therm model and the state-of-the-art methods.

5 Conclusion

In this work, we propose a lightweight and computationally efficient data-driven LIB thermal model based on KAN architecture to accurately estimate the battery core temperature. This proposed KAN-Therm model leverages the learnable activation functions of KAN to efficiently learn the nonlinear relationship of the battery core temperature using the battery surface temperature, coolant temperature, coolant flow rate, and current data. In this work, the final model hyperparameters were obtained through extensive grid search to ensure the best performance in terms of accuracy, prediction time, and parameter count. When tested under both CC and dynamic charging conditions, the KAN-Therm model demonstrated better accuracy and efficiency compared to all baseline methods over all considered criteria. Specifically, KAN-Therm predictions have been 1.3 times faster, with 11% improved accuracy, and using 30% less learnable parameters in comparison to the best performing baseline ML methods among MLP, RNN, and LSTM. While the physics-based model exhibits lower parameter requirement, it required approximately 12 times more computational time compared to the proposed model. These results highlights the low memory and compute overhead coupled with the enhanced predictive capability of KAN for battery thermal management and emphasizes its suitability for deployment in resource-limited physical BMS used in safety-critical battery applications.

References

- [1] A. Bukhari, O. I. Aboulola, A. ur Rehman, A. Alharbi, W. Alosaimi, and A. Daud, “Renewable Energy Driven On-road Wireless Charging Infrastructure For Electric Vehicles In Smart Cities: A Prototype Design And Analysis,” *Energy Reports*, vol. 12, pp. 5145–5154, 2024.
- [2] D. Karnehm, A. Samanta, C. Rosenmüller, A. Neve, and S. Williamson, “Core Temperature Estimation Of Lithium-ion Batteries Using Long Short-term Memory (Lstm) Network And Kolmogorov-arnold Network (Kan),” *IEEE Transactions on Transportation Electrification*, 2025.
- [3] L. Chen, M. Hu, K. Cao, S. Li, Z. Su, G. Jin, and C. Fu, “Core Temperature Estimation Based On Electro-thermal Model Of Lithium-ion Batteries,” *International Journal of energy research*, vol. 44, no. 7, pp. 5320–5333, 2020.
- [4] X. Lin, H. E. Perez, J. B. Siegel, and A. G. Stefanopoulou, “Robust Estimation Of Battery System Temperature Distribution Under Sparse Sensing And Uncertainty,” *IEEE Transactions on Control Systems Technology*, vol. 28, no. 3, pp. 753–765, 2019.
- [5] Y. Zheng, Y. Che, J. Guo, N. A. Weinreich, A. Kulkarni, A. Nadeem, X. Sui, and R. Teodorescu, “Real-time Sensorless Temperature Estimation Of Lithium-ion Batteries Based On Online Operando Impedance Acquisition,” *IEEE Transactions on Power Electronics*, vol. 39, no. 10, pp. 13853–13868, 2024.
- [6] S. Ghosh and T. Roy, “Detection And Isolation Of Battery Charging Cyberattacks Via Koopman Operator,” *Available at SSRN 5028845*, 2024.
- [7] X. Zhang, H. Xiang, X. Xiong, Y. Wang, and Z. Chen, “Benchmarking Core Temperature Forecasting For Lithium-ion Battery Using Typical Recurrent Neural Networks,” *Applied Thermal Engineering*, vol. 248, p. 123257, 2024.
- [8] S. Zhu, C. He, N. Zhao, and J. Sha, “Data-driven Analysis On Thermal Effects And Temperature Changes Of Lithium-ion Battery,” *Journal of Power Sources*, vol. 482, p. 228983, 2021.

- [9] N. Ouyang, W. Zhang, X. Yin, X. Li, Y. Xie, H. He, and Z. Long, "A Data-driven Method For Predicting Thermal Runaway Propagation Of Battery Modules Considering Uncertain Conditions," *Energy*, vol. 273, p. 127168, 2023.
- [10] M. M. Hasan, S. A. Pourmousavi, A. J. Ardakani, and T. K. Saha, "A Data-driven Approach To Estimate Battery Cell Temperature Using A Nonlinear Autoregressive Exogenous Neural Network Model," *Journal of Energy Storage*, vol. 32, p. 101879, 2020.
- [11] N. Wang, G. Zhao, Y. Kang, W. Wang, A. Chen, B. Duan, and C. Zhang, "Core Temperature Estimation Method For Lithium-ion Battery Based On Long Short-term Memory Model With Transfer Learning," *IEEE Journal of Emerging and Selected Topics in Power Electronics*, vol. 11, no. 1, pp. 201–213, 2021.
- [12] S. Surya, A. Samanta, V. Marcis, and S. Williamson, "Hybrid Electrical Circuit Model And Deep Learning-based Core Temperature Estimation Of Lithium-ion Battery Cell," *IEEE Transactions on Transportation Electrification*, vol. 8, no. 3, pp. 3816–3824, 2022.
- [13] F. Feng, S. Teng, K. Liu, J. Xie, Y. Xie, B. Liu, and K. Li, "Co-estimation Of Lithium-ion Battery State Of Charge And State Of Temperature Based On A Hybrid Electrochemical-thermal-neural-network Model," *Journal of Power Sources*, vol. 455, p. 227935, 2020.
- [14] Y. Liu, Z. Huang, Y. Wu, L. Yan, F. Jiang, and J. Peng, "An Online Hybrid Estimation Method For Core Temperature Of Lithium-ion Battery With Model Noise Compensation," *Applied Energy*, vol. 327, p. 120037, 2022.
- [15] S. Arora, W. Shen, and A. Kapoor, "Neural Network Based Computational Model For Estimation Of Heat Generation In LiFePO₄ Pouch Cells Of Different Nominal Capacities," *Computers & Chemical Engineering*, vol. 101, pp. 81–94, 2017.
- [16] S. Yalçın, S. Panchal, and M. S. Herdem, "A CNN-ABC Model For Estimation And Optimization Of Heat Generation Rate And Voltage Distributions Of Lithium-ion Batteries For Electric Vehicles," *International Journal of Heat and Mass Transfer*, vol. 199, p. 123486, 2022.
- [17] A. Yuan, T. Cai, H. Luo, Z. Song, and B. Wei, "Core Temperature Estimation Of Lithium-ion Battery Based On Numerical Model Fusion Deep Learning," *Journal of Energy Storage*, vol. 102, p. 114148, 2024.
- [18] Y. Yang, Z. Liu, and B. Han, "Capacity Degradation Prediction Of On-road Vehicle Battery Packs By Combining Kolmogorov-Arnold With Squeeze-and-excitation Networks," *Measurement Science and Technology*, 2025.
- [19] M. H. Sulaiman, Z. Mustaffa, A. I. Mohamed, A. S. Samsudin, and M. I. M. Rashid, "Battery State Of Charge Estimation For Electric Vehicle Using Kolmogorov-Arnold Networks," *Energy*, vol. 311, p. 133417, 2024.
- [20] Y. Cui and Y. Feng, "Enhanced State Of Health Prediction For Lithium-ion Batteries Using A Hybrid Convolutional-Kolmogorov-Arnold Network," *International Journal of Electrochemical Science*, vol. 20, no. 6, p. 101008, 2025.
- [21] L. Shao, Y. Zhang, X. Zheng, R. Yang, and W. Zhou, "SOH Estimation Of Lithium-ion Batteries Subject To Partly Missing Data: A Kolmogorov-Arnold-Linformer Model," *Neurocomputing*, vol. 638, p. 130181, 2025.
- [22] H. Liu, Y. Wang, J. Wang, A. Zhang, and H. Yang, "SOH Prediction Of Battery Packs Using Dynamic Graph Convolution Combined With KAN-Driven Methods," in *2025 4th International Conference on Green Energy and Power Systems (ICGEPS)*, pp. 129–134, IEEE, 2025.
- [23] J. He, Z. Ma, Y. Liu, C. Ma, and W. Gao, "Remaining Useful Life Prediction Of Lithium-ion Battery Based On Improved Gated Recurrent Unit-generalized Cauchy Process," *Journal of Energy Storage*, vol. 126, p. 117086, 2025.
- [24] Z. Liu, Y. Wang, S. Vaidya, F. Ruehle, J. Halverson, M. Soljačić, T. Y. Hou, and M. Tegmark, "Kan: Kolmogorov-arnold Networks," *arXiv preprint arXiv:2404.19756*, 2024.
- [25] H. Chen, H. Qin, W. Chen, N. Li, T. Wang, J. He, G. Yang, and Y. Peng, "BMS: Bandwidth-aware Multi-interface Scheduling For Energy-efficient And Delay-constrained Gateway-to-device Communications In IoT," *Computer Networks*, vol. 225, p. 109645, 2023.
- [26] X. Lin, H. E. Perez, S. Mohan, J. B. Siegel, A. G. Stefanopoulou, Y. Ding, and M. P. Castanier, "A Lumped-parameter Electro-thermal Model For Cylindrical Batteries," *Journal of Power Sources*, vol. 257, pp. 1–11, 2014.
- [27] S. D. Vyas, T. Roy, and S. Dey, "Thermal Fault-tolerance In Lithium-ion Battery Cells: A Barrier Function Based Input-to-state Safety Framework," in *2022 IEEE Conference on Control Technology and Applications (CCTA)*, pp. 1178–1183, IEEE, 2022.
- [28] D. Bernardi, E. Pawlikowski, and J. Newman, "A General Energy Balance For Battery Systems," *Journal of the electrochemical society*, vol. 132, no. 1, p. 5, 1985.

- [29] D. Zhang, S. Dey, H. E. Perez, and S. J. Moura, "Real-time Capacity Estimation Of Lithium-ion Batteries Utilizing Thermal Dynamics," *IEEE Transactions on Control Systems Technology*, vol. 28, no. 3, pp. 992–1000, 2019.
- [30] S. Dey, Y. Shi, K. Smith, and M. Khanra, "Safer Batteries Via Active Fault Tolerant Control," in *2019 American Control Conference (ACC)*, pp. 1561–1566, IEEE, 2019.
- [31] R. E. Kruse and T. A. Huls, "Development Of The Federal Urban Driving Schedule," *SAE Technical Paper*, 1973.
- [32] O. Ahmadzadeh, R. Rodriguez, Y. Wang, and D. Soudbakhsh, "A Physics-Inspired Machine Learning Nonlinear Model Of Li-ion Batteries.," in *ACC*, vol. 23, pp. 3087–3092, 2023.
- [33] IEEE Dataport, "Automotive li-ion cell usage data set," 2018.
- [34] M. Claesen, J. Simm, D. Popovic, Y. Moreau, and B. De Moor, "Easy Hyperparameter Search Using Optunity," *arXiv preprint arXiv:1412.1114*, 2014.
- [35] H. H. Tan and K. H. Lim, "Vanishing Gradient Mitigation With Deep Learning Neural Network Optimization," in *2019 7th international conference on smart computing & communications (ICSCC)*, pp. 1–4, IEEE, 2019.